

Computational Study of Computed Tomography Contrast Gradients in Models of Stenosed Coronary Arteries

Parastou Eslami^{1,*}, Jung-Hee Seo^{1,*}, Amir Ali Rahsepar², Richard George², Albert
C. Lardo^{2,3}, Rajat Mittal¹

¹*Department of Mechanical Engineering, Johns Hopkins University,
Baltimore, MD, 21218*

²*Department of Medicine, Division of Cardiology, Johns Hopkins University,*

³*Biomedical Engineering, Johns Hopkins University,
Baltimore, MD, 21218*

*Authors contributed equally to this paper.

Corresponding Author:

Rajat Mittal

e-mail: mittal@jhu.edu

Phone: +1-410-516-4069

Fax: +1-410-516-7254

Total number of words of the manuscript: 6248

Number of words of abstract: 156

Number of figures: 11

ABSTRACT

Recent computed tomography coronary angiography studies have noted higher transluminal contrast agent gradients in arteries with stenotic lesions, but the physical mechanism responsible for these gradients is not clear. We use computational fluid dynamics modeling coupled with contrast agent dispersion to investigate the mechanism for these gradients. Simulations of blood flow and contrast agent dispersion in models of coronary artery are carried out for both steady and pulsatile flows, and axisymmetric stenoses of severities varying from 0% (unobstructed) to 80% are considered. Simulations show the presence of measurable gradients with magnitudes that increase monotonically with stenotic severity when other parameters are held fixed. The computational results enable us to examine and validate the hypothesis that transluminal contrast gradients (TCG) are generated due to the advection of the contrast bolus with time-varying contrast concentration that appears at the coronary ostium. Since the advection of the bolus is determined by the flow velocity in the artery, the magnitude of the gradient therefore encodes the coronary flow velocity. The correlation between the flow rate estimated from TCG and the actual flow rate in the computational model of a physiologically realistic coronary artery is 96% with a R^2 value of 0.98. The mathematical formulae connecting TCG to flow velocity derived here, represent a novel, and potentially powerful approach for non-invasive estimation of coronary flow velocity from CT angiography

Key Words: *Computational Fluid Dynamics, Coronary Computed Tomography Angiography, Fractional Flow Reserve, Coronary Artery Disease*

INTRODUCTION

Computed tomography coronary angiography (CCTA) is a diagnostic procedure to visualize the artery and specifically the lumen area of coronary arteries. The advent of high resolution multi-detector CTA (MDCTA) coupled with prospective ECG gating allows for the image scanning of the entire heart thereby enabling high-resolution assessment of the morphological details of the main coronary vessels [1]. In order to enhance the boundaries of the lumen, intravenous iodine based contrast agent is injected in to the patient. To minimize the radiation exposure and more accurately determine the optimal scan delay after the contrast agent administration in patients, the temporal variation of the contrast agent bolus (profile) is tracked at a reference location (typically at the descending aorta); the CT image is acquired when this bolus reached maximum intensity [2]. An example of MDCTA image for coronary artery with a lesion is shown in Fig 1, where the lumen is represented by gray area and HU is the Hounsfield units, which measures the level of attenuation of the X-ray beam.

In its current form, CCTA is used to identify arterial stenoses as well as to evaluate the size, shape and area-reduction due to the lesion; this information is subsequently used to make decisions on surgical intervention as well as to plan the surgery. However, this approach to angiography does not provide any information about the coronary hemodynamics (such as velocity or pressure drop across the lesion) which is a more direct measure of the functional significance of the arterial lesion and the resulting ischemia. Information on the flow has traditionally been obtained from catheterization, which is invasive and expensive.

Recent studies have raised the interesting possibility that the data from MDCTA might contain some information on the functional severity of the lesion. In particular, studies [3]–[7] have noted a continuous attenuation of contrast agent concentration along the axial direction (see Fig. 1 for example) and this attenuation gradient (termed as the transluminal contrast gradient; TCG) appears to correlate with the severity of the stenotic lesion[3]-5]. Choi et al.[4] also found that adding the attenuation gradient to the interpretation of coronary CTA improved classification of coronary artery stenosis severity, especially in severely calcified lesions. While these studies demonstrate that physiologic information could be present in the attenuation gradients noted on CCTA, the underlying mechanism of these gradients are not well understood. Furthermore, attempts at correlating TCG with well-established, indices of functional significance such as fractional flow reserve (FFR) [2] have not been encouraging [6] and it is not clear if this lack of correlation reflects an inherent disconnect between physiologic conditions and TCG, or the presence of imaging artifacts (i.e.

resolution), or inadequate control of conditions that effect the correlation between hemodynamics and TCG.

Thus, there is a need for a study that can delineate the confounding effects of physiology and imaging on TCG. Such delineation is difficult to accomplish via *in-vivo* studies firstly because the two effects (physiology and imaging) cannot be separated and secondly, imaging does not by itself provide all the information required (velocity, pressure, contrast agent distribution etc.) for determining the physiological mechanisms of TCG generation.

Motivated by this, we use computational fluid dynamics (CFD) modeling to examine the mechanism for TCG generation in stenosed coronary arteries and assess the correlation of TCG established metrics of stenotic significance. Idealized and patient-derived models of a prototypical coronary artery with stenoses varying in severity from 0% (unstenosed) to 80% (based on area constriction) are employed, and the equations of flow and contrast agent dispersion solved simultaneously in these models. The modeling approach allows a high level of control of all key parameters and variables, and provides data that facilitates the delineation of flow mechanisms from imaging artifacts. The TCG obtained from the simulations is correlated with physiologic and hemodynamic parameters and used to test our primary hypothesis regarding the mechanics for TCG generation – that TCG reflects the convection of a time-varying contrast bolus into the coronary artery, and therefore encodes information about the coronary blood flow velocity

It is important to note that to the best of our knowledge, while a number of studies have attempted to correlate TCG with measures of stenotic severity [3-6,8], none of these studies have attempted to put forth a physics-based mechanism for the generation of TCG or have obtained an strong quantitative correlation between TCG and the other hemodynamic parameters. Therefore, the significance of the present work is that we propose and validate a physical (causal) mechanism for TCG and provide a quantitative relationship between TCG and the coronary flow using computational modeling.

The implications of the findings of the current study on the diagnosis of coronary artery disease (CAD) are potentially significant. Diagnosis of CAD typically begins with a cardiac stress test which is ultimately used to help determine which patients should be referred to invasive coronary catheterization and possible coronary revascularization[9], [10]. Although a normal cardiac stress test indicates an excellent prognosis and a low incidence of major adverse cardiovascular events, stress testing has not been an adequate “gatekeeper” to the catheterization lab, as it leads to a significant number of unnecessary invasive procedures

[11] at a staggering healthcare cost and patient risk exposure. Invasive tests such as fractional flow reserve (FFR) predict those who can benefit from stents, but carry the inherent expense and risks of catheterization [12]. New diagnostic assays that combine CCTA with computational fluid dynamics (CFD) are promising [13] but involve a high degree of complexity and cost. The ability to rapidly and accurately quantify coronary hemodynamics from a standard CCTA exam, could serve as a highly potent alternative to these existing CAD diagnoses, and enable appropriate and cost-effective health care to be deployed. Such a diagnostic method could also serve as a “gatekeeper” for these invasive therapies and lead to a significant reduction in unnecessary invasive catheterization; this would not only generate significant savings in direct healthcare costs, it will also reduce the indirect costs and patient risks associated with these invasive procedure including heart attack, stroke, and death.

METHODS

Hemodynamics and Contrast Agent Transport

The blood flow inside the modeled coronary artery is assumed to be Newtonian and the hemodynamics is simulated by solving the incompressible Navier-Stokes equations,

$$\frac{\partial \vec{U}}{\partial t} + (\vec{U} \cdot \vec{\nabla}) \vec{U} + \frac{\vec{\nabla} P}{\rho} = \nu \nabla^2 \vec{U}, \quad \vec{\nabla} \cdot \vec{U} = 0 \quad (1)$$

where \vec{U} is the flow velocity, P is pressure, ρ and ν are the density and kinematic viscosity of the blood respectively. The flow in any artery is driven by the simplified transarterial pulsatile pressure drop (ΔP) and we prescribe this as an input in our both diseased and normal model as;

$$\Delta P = P_A + P_B \sin(2\pi \cdot HR / 60 \cdot t), \quad (2)$$

where HR is the heart rate in beats per minute (BPM). A Neumann type boundary condition is applied for the velocity at the inlet and exit, and a no-slip boundary condition is used on the vessel wall.

Since the volume fraction of the contrast agent is extremely low for CTA, the contrast agent can be modeled as a passive scalar[14]. The governing equation for the contrast agent concentration, C (mg/ml) is then given by;

$$\frac{\partial C}{\partial t} + (\vec{U} \cdot \vec{\nabla}) C = D \nabla^2 C \quad (3)$$

where \vec{U} is the flow velocity obtained from the solution of Eq. (1), D is the molecular diffusivity of the contrast agent in the blood. This model has been used for the simulation of

contrast agent dispersion in many previous studies[9–11]. Interestingly, the diffusivity of the contrast agent in the blood is not well characterized and past studies have employed Schmidt numbers ($Sc = \nu/D$) ranging from 1 to 1000 [14], [15]. In the present study, we use $Sc=1$ and the effect of Sc on the TCG will be discussed in the later section. Given that contrast is excluded from the intracellular space and thus should not cross the coronary endothelium, a zero wall flux boundary condition for the contrast agent is applied as an approximation to the actual physics on the lumen boundary. This is also consistent with previous computational models of contrast transport in arteries [9]. Furthermore, we employ a convective outflow boundary condition at the downstream ends of the arteries. The boundary condition at the inlet is more complex and is described in the following section.

Arterial input function

The time-variation of the contrast agent concentration at the coronary ostium, referred to here as the “arterial input function,” (AIF) is a key factor that effects contrast agent gradients, and needs to be prescribed as an input in the model. In the automated bolus triggering method typically employed in CCTA, the attenuation level is tracked at a reference position in the aorta, and the final image acquisition scan triggered at some prescribed HU level (300 HU in Figure 2a) which is usually at or near the peak of the bolus. This data is typically discarded in a standard CTA acquisition but as has been shown recently, the AIF can be used to improve myocardial CT perfusion measurements[17]. Figure 2a shows an AIF captured at the descending aorta in a patient with coronary artery disease undergoing clinical CTA. This shows a smooth rise from a nominal value of about 50 to a peak value of about 350 to 400 HU, at which point the image is acquired. The scanner is triggered at around 300 HU in the current protocol and the volume images are acquired 1-2 heart beat after. Figure 2b represents the AIF in a canine model in which a smooth but rapid ride to maximum as the bolus arrives in the aorta similar to human studies, followed by a slow decay reflecting the flushing out of the contrast agent bolus. The typical time-delay between arrival of the bolus and maximum enhancement in human studies ranges from 10 to 15 seconds. Given the fact that the attenuation at the descending aorta is not significantly different from the value at the coronary ostium (aortic root), and the attenuation in Hounsfield units (HU) is directly proportional to the contrast agent concentration C [17], the recorded AIF shown in Fig. 2a can be used for the inlet boundary condition of the contrast agent. In order to model this, we prescribe the arterial input function in terms of concentration, C as

$$C_{ostium}(t) = C_{min} + \frac{1}{2}(C_{max} - C_{min}) \left(1 - \cos \frac{\pi(t-t_s)}{T_d} \right) \quad (4)$$

where C_{max} and C_{min} are the maximum and minimum concentrations at the ostium, t_s is the arrival time of the bolus, and T_d is the time-delay between the arrival of the bolus and the maximum enhancement. This function provides a reasonable representation of the actual time-variation of attenuation in patients as shown in Fig. 2a and we choose $T_d=10-20$ (sec) for our simulations. Note that the modeling of the contrast agent dispersion starts at $t=t_s$ and continues till $t=t_s+T_d$ and the distribution of the contrast agent (and associated attenuation) in the artery examined at $t=t_s+T_d$. We also note here that other functions (such as for instance, linear with time) could also be used to represent the AIF; this would not change the essential features of the mechanism proposed here but would change the precise form of the mathematical formulae that are derived in later sections.

Arterial attenuation and TCG calculation

As shown in Fig. 1, TCG is derived from the axial variation of cross-sectional averaged attenuation. The attenuation averaged over the cross sectional lumen area at a given axial location, s (mm) (see Fig. 3), at any given time instance normalized by the maximum attenuation increase at the coronary ostium is given by

$$HU^*(s) = \frac{HU(s)}{HU_{max} - HU_{min}} = \frac{\bar{C}(s)}{C_{max} - C_{min}}; \quad \bar{C}(s) = \frac{1}{A(s)} \int_{A(s)} C dA \quad (5)$$

where $A(s)$ is the cross-sectional area. Note that in the above, we denote the attenuation in terms of the Hounsfield Units (HU) as is traditionally done in CT imaging [4]. The assumption here is that the attenuation is linearly proportional to the contrast agent concentration [18]. The contrast agent attenuation is computed at 2 mm intervals along the artery and the normalized transluminal contrast gradient (TCG*) is estimated as the slope of the linear regression fit to this normalized transluminal attenuation profile. For example, if the profile is fit to the linear function as $HU^*(s)=a*s+b$, then TCG* is given by the slope a , and its unit is (mm^{-1}). The spatial resolution chosen does not affect the results since a linear regression has employed and is the resolution is chosen to be close to the value of 5 mm which is typical for new scanners

Fractional flow reserve

While there are a number of metrics/indices proposed for evaluating the functional significance of arterial lesions, fractional flow reserve (FFR) has emerged as the gold standard for the assessment of the functional significance of arterial stenoses[19]. As such, some recent studies have attempted to correlate TCG with FFR[3],[20]. In the current study, we use the fractional flow reserve based on the flow rate (FFR_Q) as a functional measure of the severity of coronary stenosis[19]. The flow-rate based FFR is defined by $FFR_Q = Q_s / Q_n$, where Q_s is the flow rate in the stenosed artery at the hyperemic condition, and Q_n is the hyperemic flow rate in the same artery without the stenosis. FFR_Q is readily available from our computational model since we simulate the flow in both the stenosed and unstenosed arteries. We note that FFR is in practice measured at hyperemic conditions to minimize the myocardial resistance and distinguish the effect of the stenosis resistance. However in our models (which is an idealized coronary artery segment) since we are not modeling the resistance of the myocardial capillary network, we cannot model the induction of hyperemia. Thus, our approach might not reproduce the numerical values of FFR typically measured in clinical settings; however it is expected that the trends in FFR with stenotic severity and correlation with TCG should be recovered reasonably well.

Analytical investigation of mechanism for TCG

The dispersion of contrast agent is governed by the convection-diffusion equation, Eq. (3). For a simple pipe flow, the equation for axial gradients of the cross-sectional area-averaged concentration, \bar{C} (which is directly connected with TCG, see Eq. 5) can be written as

$$\frac{\partial \bar{C}}{\partial s} = -\frac{1}{\bar{U}} \frac{\partial \bar{C}}{\partial t} + \frac{1}{\bar{U}} \left(D + \frac{d^2 \bar{U}^2}{B \cdot D} \right) \frac{\partial^2 \bar{C}}{\partial s^2} \quad (6)$$

where $\bar{U} = Q / A$, s is the axial distance, d is the diameter of the pipe. The first term on the right hand side of Eq. (6) is the advection of the input bolus (i.e. AIF) and the other terms are the axial molecular diffusion and the Taylor dispersion effects [21] which is caused by the non-uniform cross-sectional velocity profile. For a parabolic velocity profile, the constant B in the Taylor dispersion term can be evaluated analytically and is equal to 192.

Now we apply scaling analysis to each term on the right hand side of Eq. (6). From Eq. (4), since the concentration varies by $\Delta C = C_{\max} - C_{\min}$ over T_d , the order of magnitude of the first term on the right-hand-side is $O(\Delta C / (T_d \bar{U}))$, and if we take $(T_d \bar{U})$ as the axial

length scale, the orders of magnitude for molecular diffusion and Taylor dispersion are given by $O(\Delta C \cdot D / (T_d^2 \bar{U}^3))$ and $O(\Delta C \cdot d^2 / (T_d^2 \bar{U} \cdot BD))$, respectively. If the typical values for the LAD coronary flow ($\bar{U}=10$ cm/sec[22], $T_d=10$ sec, $d=3$ mm[23]) are substituted, the ratio of molecular diffusion and Taylor dispersion effects to the bolus propagation effect are $4 \times 10^{-5} / Sc$ and $10^{-3} \times Sc$, respectively (Sc is the Schmidt number, $Sc=\nu/D$). Thus, molecular diffusion effects are negligible compared to the advective effect even for small ($O(1)$) values of the Schmidt number. Taylor dispersion effect would be comparable to advective effects for $Sc=O(10^3)$, but for this regime, the assumption for the Taylor dispersion formulation (radial variation of C is much smaller than \bar{C}) will not hold. Actual CCTA data (Fig. 1) suggests that the Schmidt number for the contrast agent may not have such a high magnitude since the contrast shows a rather weak variation in the radial direction. Thus we hypothesize here that advection effects are dominant and TCG is therefore a reflection of the advection of the contrast bolus at coronary ostium.

By assuming that the contrast agent dispersion in axial direction is dominated by the advection, and considering axial variation of cross-sectional area, $A(s)$, the equation for \bar{C} can be written as

$$\frac{\partial \bar{C}}{\partial t} + \frac{Q}{A(s)} \frac{\partial \bar{C}}{\partial s} = \frac{\partial \bar{C}}{\partial t} + Q \frac{\partial \bar{C}}{\partial \eta} \approx 0, \quad (7)$$

where $\eta = \int A(s) ds$. The solution of Eq. (7) is given by

$$\bar{C}(t, s) \approx C_{ostium}(t - V(s) / Q), \quad (8)$$

where $V(s) = \int_0^s A(s) ds$ and C_{ostium} is the time variation of concentration at $s=0$, i.e the arterial input function (AIF). The normalized TCG (TCG^*) can be given by the slope of linear regression line for $\bar{C}(t, s) / \Delta C$, where $\Delta C = C_{max} - C_{min}$. Based on the mean value theorem, the slope is given by

$$TCG^* = \frac{1}{\Delta C} \frac{\bar{C}(s_b) - \bar{C}(s_a)}{s_b - s_a} = \frac{1}{\Delta C} \frac{\partial \bar{C}}{\partial s}(\hat{s}), \quad (9)$$

where s_a and s_b are the axial locations where $\bar{C}(t, s) / \Delta C$ intersects with the linear regression line, and $s_a \leq \hat{s} \leq s_b$ and is the local axial direction along the vessel which is located at the section of interest where TCG is measured (i.e. TCG^* is represented by the linear slope between the proximal (s_a) and distal (s_b) points.)

. From Eqs. (7) and (8), we get

$$\text{TCG}^* \approx -\frac{1}{\Delta C} \frac{A(\hat{s})}{Q} \frac{\partial \bar{C}}{\partial t}(\hat{s}) \approx -\frac{1}{\Delta C} \frac{A(\hat{s})}{Q} \cdot \frac{\partial}{\partial t} C_{ostium}(t - V(\hat{s})/Q). \quad (10)$$

Thus TCG^* is inversely proportional to the flow rate, Q , but also related with the arterial input function, $C_{ostium}(t)$. Substituting in the AIF used in the present study (Eq. 4) into Eq. (10), the TCG^* at $t=t_s+T_d$ is estimated as

$$\text{TCG}^* \sim -\frac{1}{2} \frac{A(\hat{s})}{Q} \frac{\pi}{T_d} \sin\left(\frac{\pi V(\hat{s})}{T_d Q}\right) \approx -\frac{1}{2} \left(\frac{1}{Q^2}\right) \left(\frac{1}{T_d^2}\right) \pi^2 A(\hat{s}) V(\hat{s}). \quad (11)$$

For the typical values for the coronary flow, the term inside the sine function in Eq.(11) is $\sim O(0.1)$ and thus it can be approximated as shown above. Most interestingly, this expression clearly suggests the correlation between the TCG and a key hemodynamic variable; the coronary flow rate Q as $\text{TCG}^* \sim 1/Q^2$. The expression, Eq. (11) and the present hypothesis will be verified by the simulation for the model coronary artery. Fig. 2C is a schematic that illustrates the analytical mechanism described: TCG is the transluminal (spatial) projection of the time profile of the contrast agent and hence is driven by the coronary blood flow velocity (V_{CF}). Therefore, comparing to the stenosed vessel, the higher flowrate (and velocity) in the normal vessel will have a lower TCG values and vice versa (Eq. 11).

Quantitative Flow rate Estimation using TCG

Equation (11) provides the basis for the non-invasive estimation of coronary blood flow rate using the contrast agent gradients, since all other variables in the equations are known from the CCTA. To estimate the blood flow rate through the vessel, Q , Eq. (11) can be re-written as;

$$Q_{TAFE} \approx \frac{\pi}{T_d} \sqrt{\frac{A(\hat{s})V(\hat{s})}{-2 \cdot \text{TCG}^*}}. \quad (12)$$

and we refer to the above method of determining the flow rate as Transluminal Attenuation Flow Encoding (TAFE). The vessel cross-sectional area, A , volume V , and normalized TCG are all available on the CCTA data, and T_d can be obtained from the AIF. The above equation is derived for a single vessel, while the real coronary artery has many branches. The above method can however be extended for a branched arterial network. Consider a branched artery network shown schematically in Fig 4A. If we apply the convection equation, Eq. (7) to the main branch connecting segments S_1, S_2 , and S_3 , the solution for the contrast agent profile at the axial location on the segment 3, for example, will be;

$$\bar{C}(t, s) \approx C_{ostium} \left(t - \frac{V_3(\hat{s})}{Q_3} - \sum_{j=1}^2 \frac{V_j}{Q_j} \right), \quad (13)$$

where Q_j and V_j are the flow rate and volume for the segment j , respectively. Basically, Eq. (13) is a modification of Eq. (8) based on the fact that the flow rate through the each segment is different. Thus, the normalized TCG measured on the each arterial segment is related to the AIF by;

$$TCG_n^* \approx -\frac{1}{\Delta C} \frac{A_n(\hat{s})}{Q_n} \cdot \frac{\partial}{\partial t} C_{ostium} \left(t - \frac{V_n(\hat{s})}{Q_n} - \sum_{upstream} \frac{V_j}{Q_j} \right), \quad (14)$$

where the summation on the last term is for the all the upstream segments back to the coronary ostium. For example, if $n=3$, the summation for the upstream should include the segments 1 and 2. Using Eq. (14), the flow rate through the segment n , Q_n can be estimated using TCG_n^* as;

$$Q_n = \frac{\tau + \sqrt{\tau^2 + 4 \cdot TCG_n'' \cdot V_n(\hat{s})}}{2 \cdot TCG_n''}, \quad (15)$$

where

$$TCG_n'' = \frac{-2 \cdot TCG_n^* T_d^2}{A_n(\hat{s}) \pi^2} \quad \text{and} \quad \tau = \sum_{upstream} \frac{V_j}{Q_j}, \quad (16)$$

where TCG'' is the regulated TCG and τ is the branch retarded time which is the time delay between the coronary ostium and the proximal branching point of the vessel segment. Note that to evaluate τ , the flow rate through all the upstream vessel segments should be known. Thus, Eq. (15) should be applied from the most upstream segment to estimate the flow rate sequentially.

RESULTS

Idealized Model

The first objective here is to understand the fundamental mechanism for TCG generation as well as the effect of features such as flow velocity, bolus duration and arterial bifurcations, which are expected to have a bearing on flow, contrast agent dispersion, and therefore TCG. This is best accomplished with a simple and idealized model of a coronary artery used in this component of the computational study as shown in Fig. 4. The length of the main artery in this model is 20 cm; the proximal and distal diameter of this artery are 4mm and 2 mm

respectively and a linear taper with angle equal to 0.29 degrees is employed. In order to mimic the effect of branching on flow and contrast gradients, we have included two branches from the main vessel; these are located at 16% and 57.5% of the length of the main vessel. The proximal diameters of these vessels are approximately 3.2 mm and 2.3 mm and the taper angles are 0.16 and 0.10 degrees respectively. We note at the outset that while the topology and dimensions of the model are based generally on a typical left coronary artery, the model is not derived from any patient-specific data and is not anatomically-exact. For the cases with stenosis, axi-symmetric stenoses are created on the main artery segment between the two bifurcations (Fig. 4B). The stenosis extends about 10 mm in the axial direction and the severity (based on area reduction) varies from 50 to 80%.

In order to understand the effect of flow rate on TCG, two different mean flow rate conditions are modeled by choosing $P_A = 3.0$ and 4.5 mmHg and $P_B=0$ for both flow cases. For the pulsatile flow conditions $HR=60$ BPM and $P_B = 2.85$ and 4.35 mmHg are chosen for $P_A = 3$ and 4.5 mmHg, respectively. Consistent with the focus on basic mechanisms, the temporal variation of pressure is chosen to be a simple sinusoid that does not mimic the precise variation for coronary arteries. For the normal (unstenosed) artery model, the mean pressure drops of 3 and 4.5 mmHg result in mean flow rates through the main artery of $Q_n=50$ and 69 (ml/min) respectively. The mean flow velocities are $\bar{U}=11.8$ and 16.3 (cm/sec), respectively, and these are in the range of measured values for the left anterior descending (LAD) coronary arteries in rest conditions[22]. These flow conditions correspond to a mean Reynolds number ($Re=\bar{U}d/\nu$) of 88 and 122, respectively, and Womersley number ($\alpha = d\sqrt{\omega/\nu}/2 = 1.88$, where $\omega=2\pi HR/60$ is the angular frequency of the pulsatile flow and d is the artery diameter).

The results of grid refinement for both the idealized and physiological models are described in the Appendix. For the idealized model, simulations are performed for both steady and pulsatile flows with two normal mean flow rate conditions, $Q_n=50$ and 69 (ml/min), and area stenosis 50, 60, 70 and 80%. The simulations provide the pressure, velocity, and contrast agent concentration distributions for the modeled coronary arteries. The concentration in the artery is measured at the end of simulation time (10 second) when the AIF reaches its peak and this mimics the typical CCTA acquisition protocol. For example, these fields are shown in Fig. 5 for the case of steady flow, $Q_n=50$ ml/min and area constriction 70%. One can see a significant pressure drop across the stenosis and high velocity magnitudes through the stenosis.

Figure 6 shows the transluminal variation of HU^* for steady and pulsatile flow cases with normal mean flow rates, $Q_n=50$ and $Q_n=69$ (ml/min). All these simulations are performed with $T_d=10$ (sec). In these plots section (1) and (2) indicate the location of arterial bifurcations and this divides the main artery into three segments (proximal to first bifurcation, distal to first bifurcation and distal to downstream bifurcation) and results with steady flow show a characteristic piecewise linear attenuation in each of these three segments of the artery. For the pulsatile flow results, a wave-like variation is superposed on the linear distribution of attenuation. It is observed, however, that the magnitude of the attenuation gradient increases constriction size in all segments of the artery.

Values of TCG^* are estimated for the intermediate segment of the artery (segment that lies between points (1) and (2) denoted in Fig. 6 by linear regression as described in the methods section, and Figures 6A and 6B show the variation of TCG^* with area constriction for the steady and pulsatile flows with two different mean flow rate conditions. We note that while the magnitude of TCG^* does increase with increasing constriction, the value of TCG^* also depends on the flow rate conditions and decreases in magnitude as the flow rate increases.

Analytical investigation of TCG formation in Eq. (11) suggests the relations; $TCG^* \sim 1/Q^2$ and $TCG^* \sim 1/T_d^2$. These correlations are examined in Fig. 7 for the current simulation results. Figures 7A and 10B show that TCG^* has a strong ($R>0.92$) linear relationship with $1/Q^2$ for both steady and pulsatile flows. In order to assess the effect of T_d , we performed additional simulations for 70% stenosis, $Q_n=50$ ml/min with T_d varying from 10 to 20 (sec) in the steady flow case. The results are plotted in Fig. 7C, which indicates a clear linear relationship between TCG^* and $1/T_d^2$ ($R=0.99$). Thus, the results shown in Fig. 7 seem to verify our hypothesis on the mechanism of TCG generation and the expression, Eq. (11). It is interesting to note that though Eq. (11) has been derived for the idealized steady pipe flow, the correlation between TCG and the coronary flow rate, Q still holds for the unsteady pulsatile flow through a relatively complex model of a coronary arteries. Figures 7D show plots of TCG^* versus FFR_Q for both flow rate conditions and it is noted that the magnitude of TCG^* decreases with increasing FFR_Q . However, the correlation between TCG^* and FFR_Q is significantly affected by the flow rate condition and is relatively poor ($R=0.41$).

Physiological Model Based on Coronary CT

From the previous section, the correlation between the inverse of flow rate squared and TCG* is clear. To prove that the same mechanism holds for a more realistic model, the same steady computation has been performed for the normal case and 70% stenosis. The normal case geometry (Fig. 8A) has been generated from a patient specific data from CTA images and a 70% stenosis (Fig. 8B) has been created manually using the normal geometry to compare the two cases. There were no regions of calcification in the artery of interest for this subject, thereby enabling acquisition of a high-quality image throughout the vessel of interest. The study has been modeled such that the mean flow rate through LCA matches the stress condition in clinical measurements. Therefore by choosing PA=3.0 mmHg, the mean flow rate in LCA will be $Q_n = 375$ (ml/min) which is within the range of measured values of left coronary arteries [22]. The mean flow velocity is $\bar{U} = 25.1$ (cm/sec) which would correspond to the mean Reynolds number $Re = \bar{U}d/\nu = 454$.

Figure 9 provides the simulation results for the pressure, velocity, and contrast agent concentration distribution for the mentioned flow rate of $Q_n = 375$ (ml/min) and the area constriction of 70%. As expected, a pattern similar to the idealized case can be observed in the patient derived model which includes a significant pressure drop across the stenosis along with high velocity magnitudes through the stenosis. Figure 10A shows the transluminal contrast agent concentration HU* for both the no-stenosis and 70% stenosis cases where the section S₁-S₄ has been defined along the main LAD before each branch point (Fig. 9A). The values of TCG* are estimated as described earlier in the paper. Based on the analytical relation between TCG* and the flow rate Q_{TAFE} , Eq. (12), the flow rates were estimated. Figure 10B demonstrates a strong correlation with an $R^2 = 0.98$ between the flow rate estimate by TAFE and the one obtained in the CFD calculation, for both the normal and 70% area stenosis cases for different sections of S₁ to S₄.

DISCUSSION

In this paper, the mechanism for the generation of contrast agent gradients in coronary arteries observed in cardiac CT has been investigated via computational fluid dynamics simulation and the analysis of the convection-diffusion equation. The current simulations of blood flow and contrast agent dispersion in models of stenosed coronary arteries show that TCG is measurably higher in arteries with a constriction and that TCG is correlated with coronary flow velocity, which in these models, is associated with different stenotic severities.

Although CFD has its own limitation associated with modeling and discretization errors, the exclusion of imaging artifacts and the capability to precisely control the boundary conditions and other features (e.g., arterial geometry, trans-arterial pressure drop and arterial input function) in the current modeling study allows us to suggest that TCG does indeed encode information that is intrinsically related to coronary flow. The analysis of the convection-diffusion equation for the contrast agent also provides insight into the mechanism responsible for TCG

More specifically, axial or transluminal varying contrast agent concentration is induced by the advection of the time-varying contrast agent bolus that enters at the coronary ostium. Given the typical temporal profile of the arterial input function and the acquisition of the image at or near the time corresponding to maximum enhancement at the ostium, this necessarily implies that the contrast agent concentration imaged at this time-instance will show a decrease from the ostium to the distal segment of the artery.

The analysis also suggests that the flow velocity in the artery will clearly affect the overall gradient in the contrast agent concentration; a higher velocity will tend to “stretch” (and therefore decrease) the contrast agent gradient whereas a lower flow velocity will tend to steepen (and increase) the gradient. Similarly, for longer T_d , the contrast agent gradient is stretched further, thus TCG decreases. This is confirmed quantitatively by the strong correlation between TCG and the coronary flow rate ($TCG^* \propto 1/Q^2$) as well as between TCG and the bolus duration ($TCG^* \propto 1/T_d^2$) that are suggested in Eq. (11). We reiterate here that a different fit to the bolus (such as for instance, linear with time) would lead to a different correlation but not change the fundamental physical mechanisms hypothesized here.

The higher TCG* magnitude for higher area-stenosis is therefore due to the fact that for a given axial pressure drop, increase in constriction size increases flow resistance, and reduces the flow rate, which is correlated with a higher gradient. This issue will be discussed later in this section when describing the correlation between TCG* and FFR. The mechanism also explains the increase in the gradient at the two bifurcations evident in Fig. 6; each bifurcation siphons flow away, thereby reducing the flow rate through the main branch and this leads to a steepening of the attenuation gradient distal to the bifurcation.

It is noted that since the model adopted here does not account for the microvascular resistance, which is dominant during physiologic rest conditions, the velocity drop associated with the area reduction for a given stenosis is significantly exaggerated here. It is well known that significant reductions in resting coronary flow rates only occur for very severe (> 95% area) stenoses and that for less severe lesions, the reductions in rate-of-flow are quite small

[24]. Thus, the current results should not be taken to imply that TCG or related contrast information could be used to identify and/or stratify the reductions in flow-rates associated with intermediate stenoses. Rather, the current results primarily point to the causal relationship between TCG and flow rates.

The dependency of the measured TCG on the arterial input function has significant implications for *in-vivo* measurement of TCG. In most studies to date [3]–[5], [8] no particular attention has been given to controlling (or for that matter, even recording) the arterial input function. It is clear from our simulations that the value of TCG is very much dependent on the duration of bolus buildup in the coronary ostium ($TCG^* \sim 1/T_d^2$), and analysis also indicates that it is also dependent on the AIF profile (see Eq. 10). Thus, a raw value of TCG that does not account for (or compensate for) the duration of the arterial input function is expected to have relatively low prognostic value. Equation (11) also indicates that the precise value of TCG is affected by the cross-sectional area, A and the volume of arterial segment up to the position where the measurements are made. Lack of compensation for these additional factors is likely to further decrease the correlation between TCG and coronary flow measured *in-vivo*. It is important to note that as per Eq. (11), the axial variation of cross-sectional area (i.e. area gradient, $dA(s)/ds$) does not play a role in the TCG formation.

The data obtained from the current simulation show that while TCG is monotonically correlated with FFR_Q the overall correlation between the two is low ($R=0.41$). However, even with a high degree of control of the AIF and the absence of imaging artifacts, the correlation between TCG and FFR is confounded by the baseline flow conditions in the artery. Note that there are a wide variety of factors that can affect the baseline flow rate through the coronary arteries of a patient which include (but are not limited to) overall cardiac health and medication (such as adenosine). All of these differences will be reflected in the TCG value (which encoded for flow velocity) but not in the FFR. All of the above analysis underscores the difficulty of correlating TCG to functional measures of stenoses such as FFR, and might explain the moderate to poor correlation ($R=0.39-0.43$) between the attenuation gradient and FFR reported in the previous *in-vivo* studies[25]. In addition to the confounding effects of the arterial input function and imaging artifacts, this correlation is highly affected by the flow rate conditions, which may vary significantly from patient to patient.

The coronary artery models used in the current study are well suited for the fundamental analysis carried out here but they have a number of potential limitations. First, the use of a prescribed pressure drop across the vessel and with no capillary resistance introduced at the vessel outlet is not a precise representation of the physiological situation. In particular, this tends to amplify the effect of the stenosis on the flow rate and FFR, and this is something that is observed in the data (see Fig. 7). However, this should not affect the primary objective and observation of the study, which is that TCG is inversely related with the effect that vessel stenosis has on the flow rate. Second, the shape of the stenoses are generated via a parametric formula and do not correspond to a naturally occurring lesions. Third, the arterial input function applied at the coronary ostium of the current model (see Fig. 8) is actually based on measurements in the mid descending aorta. While there will be some differences in the contrast agent buildup at the two locations, we do however expect that the two profile shapes and trends would be quite similar. Nevertheless, this issue needs to be investigated in a future study. Fourth, in the cases of presence of any imaging artifacts such as temporal and spatial resolutions and calcification or stents inside the diseased vessel, TCG will get affected and hence the estimated flow rate as well. One way to eliminate this artifact is to eliminate the segment with calcification or stent from TCG measurements; this is the subject of ongoing studies. Finally, the effect of a physiological coronary flow waveform and the prescribed pressure on the attenuation function and TCG is currently being studied and these results will be reported in the future.

It is also useful to discuss a seeming discrepancy between our simulation results and the TCG measured in-vivo: our simulations show only a 2-15% drop of the normalized HU (HU^*) over the entire length of the vessel, whereas the clinical example (Fig. 1) shows about a 75% drop. As indicated in Eqs. (9) and (10), the overall drop of HU^* over the vessel depends directly on the temporal change of HU in the AIF (or dC/dt), which can vary significantly with the precise shape of the AIF as well as the time-point in the AIF when the CT image is acquired. For example, in the AIF shown in Fig. 2A, the rate of change near the AIF maximum (where the current analysis is done) is about 5 HU/sec while the maximum (in the middle of AIF) is about 30 HU/sec. Thus, a change in the timing of the acquisition could create a six-fold or more increase in the magnitude of the measured TCG. In this regard, it is noted that past studies have not appreciated this connection between AIF and TCG, and the current analysis provides a physical, as well as mathematical basis for such insights into TCG. In addition to the above factors, imaging artifacts in CT imaging (which are not included in the current computational model), particularly partial-volume averaging

(PVA) effects, also contribute significantly to the measured TCG in the vessels. The relative contribution of PVA to TCG depends on a number of factors including scanner resolution (pixels per diameter), the coronary flow velocity and vessel taper, and in some cases, might provide a dominant contribution to TCG. However, we have recently developed mathematical formulation to correct TCG for PVA effects, and the application of this formulation to CCTA data will be presented in a future paper.

In summary, while all of the above simplifications and assumptions are expected to affect the precise numerical value of TCG, we do not expect them to alter the basic mechanism that has been put forth by the current study: that transluminal contrast gradients exhibit the effects of the advection of the AIF into the artery and they encode the coronary flow velocity. This basic mechanism has been discussed and confirmed in recent clinical and preclinical studies [26]–[28].

CONCLUSIONS

Computational modeling of flow and contrast dispersion has been used to explore the hypothesis that transluminal contrast gradients are formed due to the advection of the time-varying contrast bolus that arrives at the coronary ostium. According to this hypothesis, a higher velocity in the coronary vessel will tend to “stretch” (and therefore decrease) the contrast agent gradient whereas a lower flow velocity will tend to steepen (and increase) the gradient. Simulations for both an idealized model as well as a physiologically realistic coronary artery model confirm the above hypothesis and show that these contrast gradients encode for the coronary flow velocity. All other conditions being the same, our mathematical analysis and simulations show that a larger stenotic blockage reduces flow velocity which increases the gradient, and might explain the correlations between stenotic severity and TCG observed in previous studies. The mathematical analysis of dispersion also reveals that the bolus duration is a key parameter that relates these gradients to the flow velocity. The mathematical formulae connecting TCG to flow velocity derived here, represent a novel approach for non-invasive estimation of coronary flow velocity from CT angiography and should also facilitate investigations and analyses of these gradients that are grounded in the physics of flow and dispersion.

ACKNOWLEDGEMENT & CONFLICT OF INTEREST

RM, RTG, & ACL would like to acknowledge support from the Coulter Foundation for this work. Some of the authors of the papers are named inventors on patents (pending) in the area of contrast agent gradient based assessment of blood flow. RM and ACL have other significant financial interests in technologies associated with contrast agent gradient based flow assessment. RTG and ACL report research support from Astellas Pharma. RTG also reports research support from General Electric, Toshiba Medical Systems Corporation, and Caprior, Inc. RTG is a consultant for ICON Medical Imaging. The terms of these arrangement are being managed by Johns Hopkins University in accordance with its conflict of interest policies.

APPENDIX: GRID RESOLUTION STUDIES

Idealized Model

The simulations are conducted using COMSOL™ 4.3 which is an unstructured, finite-volume-based solver. The coronary artery model is discretized with a total of about 2.5×10^5 tetrahedral elements (Fig. 4C) based on a mesh refinement study. In particular, simulations on a significantly finer mesh with 6×10^5 elements produces at most a 6% difference in the mean flow-rate and 3% in the peak flow rate through the main artery indicating effective grid convergence. The time solver was set to use the Generalized-Alpha Method which is second order accurate [29] and the time-step is chosen according to the physical geometry and not to exceed 0.01 seconds. The solver uses V-cycle second order multigrid for the advection scheme.

Physiological Model

The patient derived model simulations are conducted using ANSYS™ Workbench 14.5. The left coronary artery model is discretized with an unstructured mesh with total of approximately $\approx 4.55 \times 10^5$ tetrahedral elements (Fig. 8C). Fig. 11A illustrates the velocity magnitude profile taken at the same cross sectional line (Fig. 11B) for 4 different grid levels of ‘Coarse’ with $\approx 2 \times 10^5$, ‘Normal’ with $\approx 3 \times 10^5$, ‘Fine’ with $\approx 4.55 \times 10^5$ and ‘FineR’ with $\approx 9.25 \times 10^5$ tetrahedral elements. This figure illustrates a minimal difference in the peak velocity profile between the Fine and FineR grids; hence all the simulations have been conducted using the ‘Fine’ grid. The time solver chosen employed a second order backward

Euler scheme with a step size of $\Delta t=0.01$ sec and the high resolution scheme described by Barth et al.[30] was used to solve the spatial partial derivatives

REFERENCES

- [1] C. R. Becker, B. M. Ohnesorge, U. J. Schoepf, and M. F. Reiser, "Current development of cardiac imaging with multidetector-row CT.," *Eur. J. Radiol.*, vol. 36, no. 2, pp. 97–103, Nov. 2000.
- [2] Vincent Ho and G. P. Reddy, *Cardiovascular Imaging- Volume 2*, 1 Har/Psc. Saunders, 2010.
- [3] J.-H. Choi, B.-K. Koo, Y. E. Yoon, J. K. Min, Y.-B. Song, J.-Y. Hahn, S.-H. Choi, H.-C. Gwon, and Y. H. Choe, "Diagnostic performance of intracoronary gradient-based methods by coronary computed tomography angiography for the evaluation of physiologically significant coronary artery stenoses: a validation study with fractional flow reserve.," *Eur. Heart J. Cardiovasc. Imaging*, vol. 13, no. 12, pp. 1001–7, Dec. 2012.
- [4] J.-H. Choi, J. K. Min, T. M. Labounty, F. Y. Lin, D. D. Mendoza, D. H. Shin, N. S. Ariaratnam, S. Koduru, J. F. Granada, T. C. Gerber, J. K. Oh, H.-C. Gwon, and Y. H. Choe, "Intracoronary transluminal attenuation gradient in coronary CT angiography for determining coronary artery stenosis.," *JACC. Cardiovasc. Imaging*, vol. 4, no. 11, pp. 1149–57, Nov. 2011.
- [5] B. J. W. Chow, M. Kass, O. Gagné, L. Chen, Y. Yam, A. Dick, and G. a Wells, "Can differences in corrected coronary opacification measured with computed tomography predict resting coronary artery flow?," *J. Am. Coll. Cardiol.*, vol. 57, no. 11, pp. 1280–8, Mar. 2011.
- [6] W. J. Stuijzfand, I. Danad, P. G. Raijmakers, C. B. Marcu, M. W. Heymans, C. C. van Kuijk, A. C. van Rossum, K. Nieman, J. K. Min, J. Leipsic, N. van Royen, and P. Knaapen, "Additional value of transluminal attenuation gradient in CT angiography to predict hemodynamic significance of coronary artery stenosis.," *JACC. Cardiovasc. Imaging*, vol. 7, no. 4, pp. 374–86, Apr. 2014.
- [7] R. Nakanishi and M. J. Budoff, "A New Approach in Risk Stratification by Coronary CT Angiography," *Scientifica (Cairo)*, vol. 2014, 2014.
- [8] M. L. Steigner, D. Mitsouras, A. G. Whitmore, H. J. Otero, C. Wang, O. Buckley, N. a Levit, A. Z. Hussain, T. Cai, R. T. Mather, O. Smedby, M. F. DiCarli, and F. J. Rybicki, "Iodinated contrast opacification gradients in normal coronary arteries imaged with prospectively ECG-gated single heart beat 320-detector row computed tomography.," *Circ. Cardiovasc. Imaging*, vol. 3, no. 2, pp. 179–86, Mar. 2010.
- [9] J. a San Román, I. Vilacosta, J. a Castillo, M. J. Rollán, M. Hernández, V. Peral, I. Garcimartín, M. M. de la Torre, and F. Fernández-Avilés, "Selection of the optimal

stress test for the diagnosis of coronary artery disease.,” *Heart*, vol. 80, no. 4, pp. 370–376, 1998.

- [10] D. Lloyd-Jones, R. J. Adams, T. M. Brown, M. Carnethon, S. Dai, G. De Simone, T. B. Ferguson, E. Ford, K. Furie, C. Gillespie, A. Go, K. Greenlund, N. Haase, S. Hailpern, P. M. Ho, V. Howard, B. Kissela, S. Kittner, D. Lackland, L. Lisabeth, A. Marelli, M. M. McDermott, J. Meigs, D. Mozaffarian, M. Mussolino, G. Nichol, V. L. Roger, W. Rosamond, R. Sacco, P. Sorlie, R. Stafford, T. Thom, S. Wasserthiel-Smoller, N. D. Wong, and J. Wylie-Rosett, “Executive summary: Heart disease and stroke statistics-2010 update: A report from the american heart association,” *Circulation*, vol. 121, no. 7, pp. 46–215, 2010.
- [11] M. R. Patel, E. D. Peterson, D. Dai, J. M. Brennan, R. F. Redberg, H. V. Anderson, R. G. Brindis, and P. S. Douglas., “Low diagnostic yield of elective coronary angiography.,” *N. Engl. J. Med.*, vol. 363, no. 1, pp. 93–94; author reply 94–95, 2010.
- [12] R. a Lange and L. D. Hillis, “Cardiology patient pages. Diagnostic cardiac catheterization.,” *Circulation*, vol. 107, no. 17, pp. e111–e113, 2003.
- [13] R. Nakazato, H. B. Park, D. S. Berman, H. Gransar, B. K. Koo, A. Erglis, F. Y. Lin, A. M. Dunning, M. J. Budoff, J. Malpeso, J. Leipsic, and J. K. Min, “Noninvasive fractional flow reserve derived from computed tomography angiography for coronary lesions of intermediate stenosis severity results from the DeFACTO study,” *Circ. Cardiovasc. Imaging*, vol. 6, no. 6, pp. 881–889, 2013.
- [14] J. Durant, I. Waechter, R. Hermans, J. Weese, and T. Aach, “Toward Quantitative Virtual Angiography: Evaluation with in vitro studies. Philips Research Europe , Aachen , Germany Institute of Imaging and Computer Vision , RWTH Aachen University , Aachen , Germany Centre for Medical Image Computing , University Coll,” pp. 632–635, 2008.
- [15] T. Kim, a Y. Cheer, and H. a Dwyer, “A simulated dye method for flow visualization with a computational model for blood flow.,” *J. Biomech.*, vol. 37, no. 8, pp. 1125–36, Aug. 2004.
- [16] F. Calamante, P. J. Yim, and J. R. Cebral, “Estimation of bolus dispersion effects in perfusion MRI using image-based computational fluid dynamics,” *Neuroimage*, vol. 19, no. 2, pp. 341–353, Jun. 2003.
- [17] A. C. A. George, Richard T;Ichihara, Takashi; Lima, Jaoa A.C.; Lardo, “A Method for Reconstructing the Arterial Input Function during Helical CT : Implications for Myocardial Perfusion Distribution Imaging,” *Radiology*, vol. 255, no. November2–May2010, pp. 396–404, 2010.
- [18] K. M. Foley WD, “Computed tomography angiography: principles and clinical applications,” *J Comput Assist Tomogr.*, vol. 27, no. Supp 1, pp. 23–30, 2003.
- [19] A. H. Bishop and H. Samady, “Fractional flow reserve: critical review of an important physiologic adjunct to angiography.,” *Am. Heart J.*, vol. 147, no. 5, pp. 792–802, May 2004.

- [20] Y. E. Yoon, J.-H. Choi, J.-H. Kim, K.-W. Park, J.-H. Doh, Y.-J. Kim, B.-K. Koo, J. K. Min, A. Erglis, H.-C. Gwon, Y. H. Choe, D.-J. Choi, H.-S. Kim, B.-H. Oh, and Y.-B. Park, "Noninvasive Diagnosis of Ischemia-Causing Coronary Stenosis Using CT Angiography: Diagnostic Value of Transluminal Attenuation Gradient and Fractional Flow Reserve Computed From Coronary CT Angiography Compared to Invasively Measured Fractional Flow Reser," *JACC. Cardiovasc. Imaging*, vol. 5, no. 11, pp. 1088–96, Nov. 2012.
- [21] G. Taylor, "Dispersion of Soluble Matter in Solvent Flowing Slowly through a Tube," *Proc. R. Soc. A Math. Phys. Eng. Sci.*, vol. 219, no. 1137, pp. 186–203, Aug. 1953.
- [22] T. Hozumi, K. Yoshida, T. Akasaka, Y. Asami, Y. Ogata, T. Takagi, S. Kaji, T. Kawamoto, Y. Ueda, and S. Morioka, "Noninvasive assessment of coronary flow velocity and coronary flow velocity reserve in the left anterior descending coronary artery by Doppler echocardiography: comparison with invasive technique.," *J. Am. Coll. Cardiol.*, vol. 32, no. 5, pp. 1251–9, Nov. 1998.
- [23] N. Funabashi, Y. Kobayashi, M. Perloth, and G. D. Rubin, "Coronary artery: quantitative evaluation of normal diameter determined with electron-beam CT compared with cine coronary angiography initial experience.," *Radiology*, vol. 226, no. 1, pp. 263–71, Jan. 2003.
- [24] K. L. Gould, K. Lipscomb, and G. W. Hamilton, "Physiologic basis for assessing critical coronary stenosis. Instantaneous flow response and regional distribution during coronary hyperemia as measures of coronary flow reserve.," *Am. J. Cardiol.*, vol. 33, no. 1, pp. 87–94, Jan. 1974.
- [25] D. T. L. Wong, B. S. Ko, J. D. Cameron, N. Nerlekar, M. C. H. Leung, Y. Malaiapan, M. Crossett, D. P. Leong, S. G. Worthley, J. Troupis, I. T. Meredith, and S. K. Seneviratne, "Transluminal Attenuation Gradient in Coronary Computed Tomography Angiography Is a Novel Noninvasive Approach to the Identification of Functionally Significant Coronary Artery Stenosis: A Comparison With Fractional Flow Reserve.," *J. Am. Coll. Cardiol.*, vol. 61, no. 12, Feb. 2013.
- [26] R. T. George, A. A. Rahsepar, P. Eslami, J. H. Seo, R. Mittal, D. Zhao, E. Guallar, L. P. Jacobson, M. Budoff, W. S. Post, and A. C. Lardo, "Abstract 17975: Coronary and Myocardial Blood Flow Measurements Derived from Coronary Computed Tomography Angiography and Transluminal Attenuation Flow Encoding in the Multicenter AIDS Cohort Study," *Circulation*, vol. 130, no. Suppl_2, p. A17975–, Nov. 2014.
- [27] F. K. K. Richard T. George, Amir Ali Rahsepar, Jung-Hee Seo, Parastou Eslami and A. C. L. Rajat Mittal, "Abstract: Application of Transluminal Attenuation Flow Encoding (TAFE) to Quantify Absolute Coronary Blood Flow," *SCCT 9th Annu. Sci. Meet.*, pp. 7–9, 2014.
- [28] A. C. Lardo, A. A. Rahsepar, J. H. Seo, P. Eslami, F. Korley, R. T. George, and A. Flow, "Computed Tomography Transluminal Attenuation Flow Encoding (TAFE): Formulation, Preclinical Validation and Clinical Feasibility," *JCCT [In Rev.]*, 2015.

- [29] J. Chung and G. M. Hulbert, "A Time Integration Algorithm for Structural Dynamics With Improved Numerical Dissipation : The Generalized-alpha Method," *ASME-Journal of Applied Mechanics*, vol. 60, pp. 371–375, 1993.
- [30] D. . Barth, T.J, Jespersen, "The design and application of upwind schemes on unstructured meshes," *AIAA Pap.*, no. 89–0366, 1989.

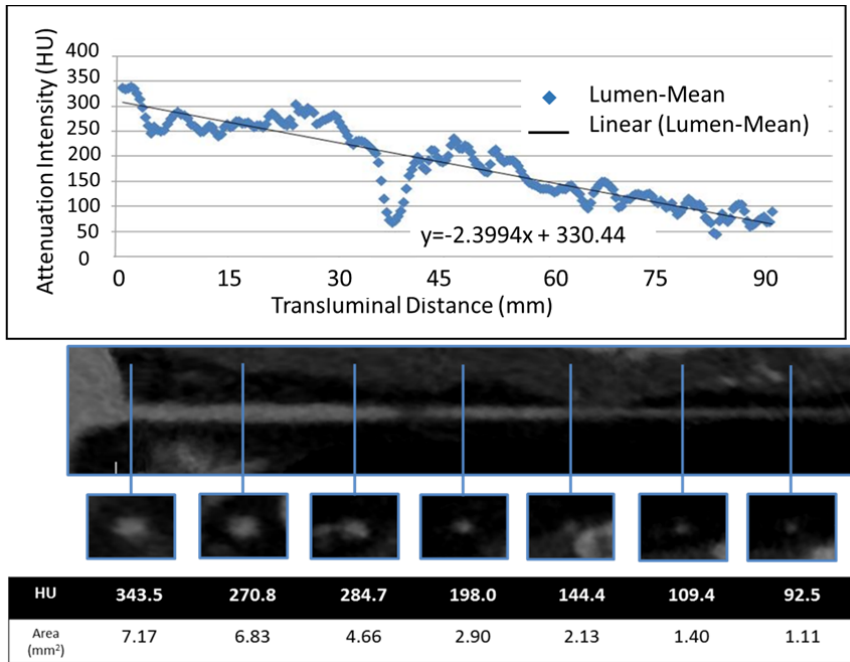


Figure 1. Representative example of transluminal contrast gradient for a stenosed artery. Luminal cross sections are sampled every 0.5 mm and plotted over the vessel length to obtain an axial variation of cross-sectional averaged attenuation (HU) (top figure). Bottom figure shows the axial and cross-sectional visualizations of lumen area by contrast agent. HU is the Hounsfield unit for the attenuation level. The lesion section is shown with an arrow. CT imaging is acquired using a 320-row detector CT scanner (AquilionTMOne -Toshiba Medical Systems Corporation, Otawara, Japan).

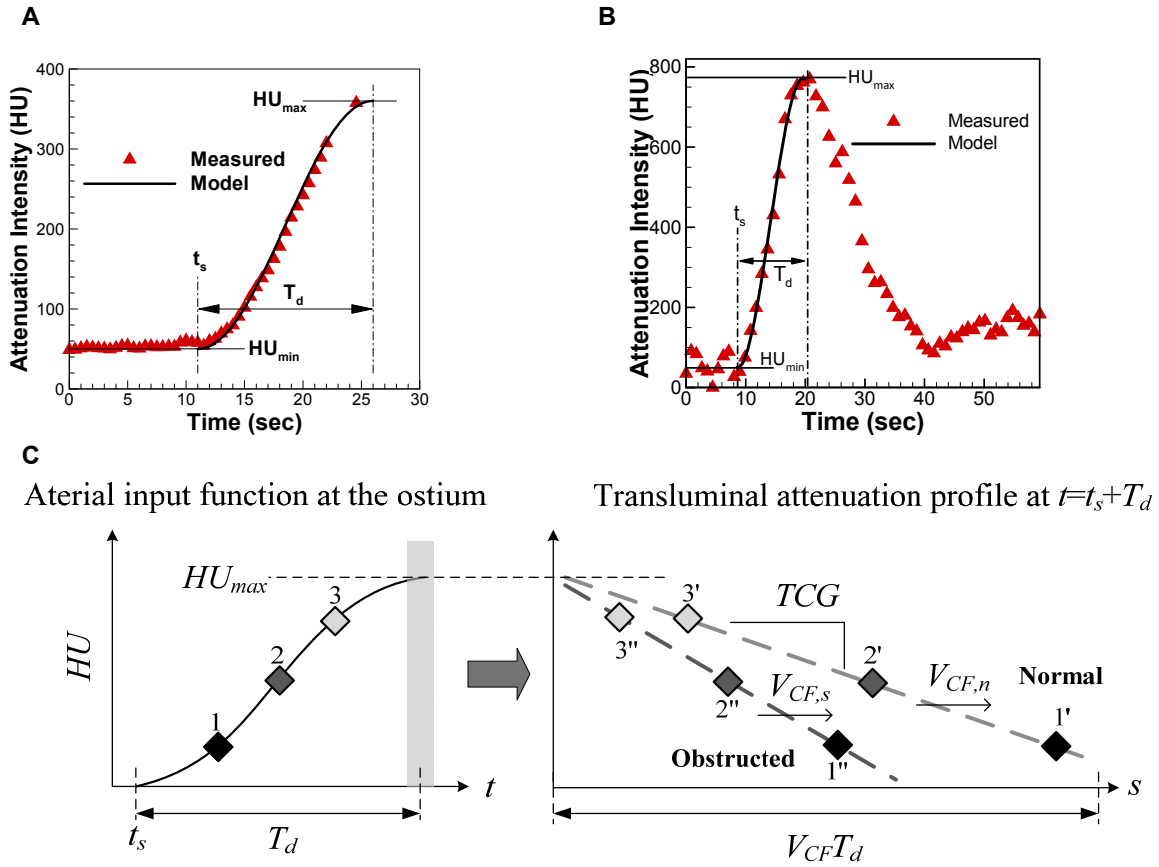


Figure 2. Representative Arterial input function (AIF) measured in actual CCTA as well as the fitted function that is employed in the simulations in a human studies (A) and a canonical study (B). Part C is a schematic to illustrate the mechanism described in the paper: TCG is the transluminal (spatial) projection of the time profile of the concentration of the contrast agent and hence is driven by the coronary blood flow velocity (V_{CF}).

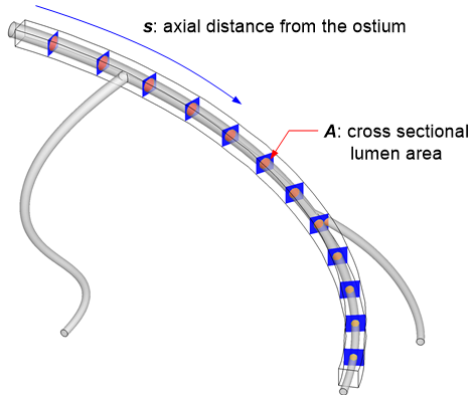


Figure 3. Extraction of cross-sectional lumen area along the axial direction from the CFD simulation for the calculation of transluminal contrast gradients.

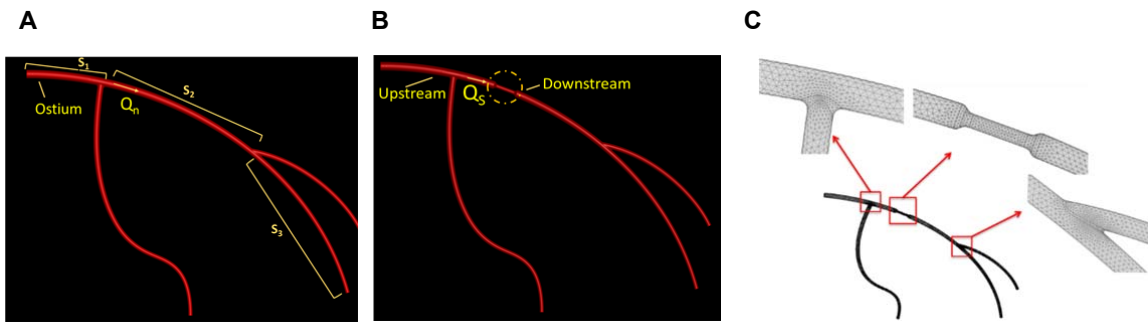


Figure 4. (A) An idealized 3-D model of the coronary artery for the normal (unstenosed) case where Q_n is referred to the normal (no stenosis) flow rate. (B) Model of the artery with a stenosis where Q_s is referred to the flow rate in the vessel with stenosis. (C) Computational meshes employed in the various segments of the model.

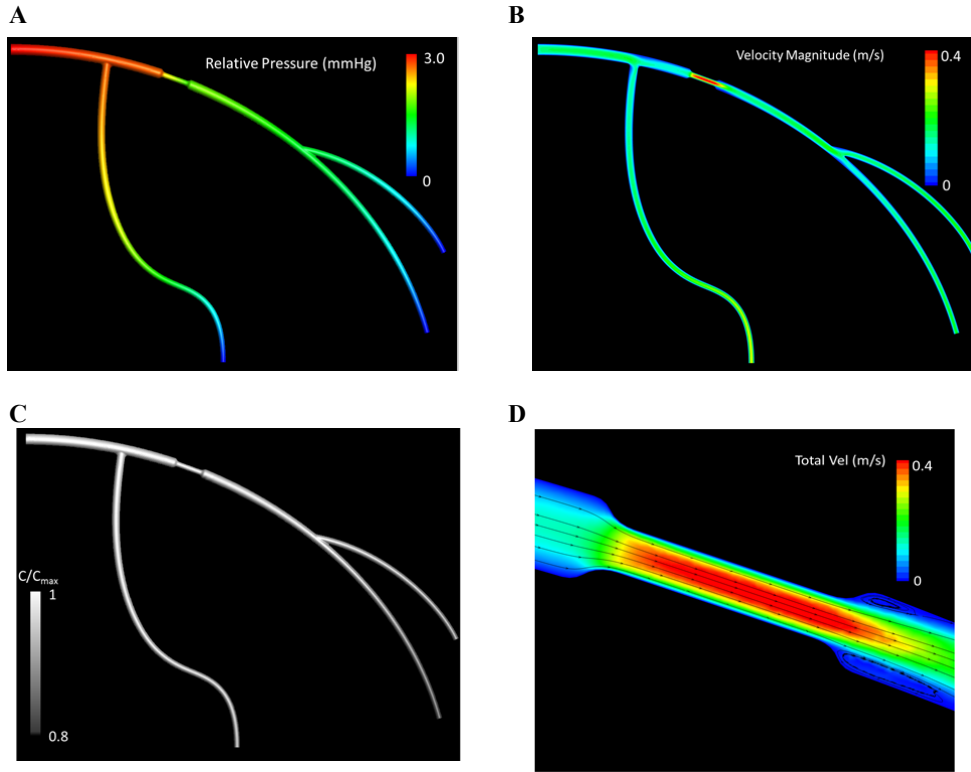


Figure 5. Pressure (A), velocity magnitude (B) and normalized contrast agent concentration (C/C_{max}) for the $Q_n=50\text{ml/min}$ case with a 70% area constriction. (D) Velocity magnitude and streamlines in the stenosed region in idealized model.

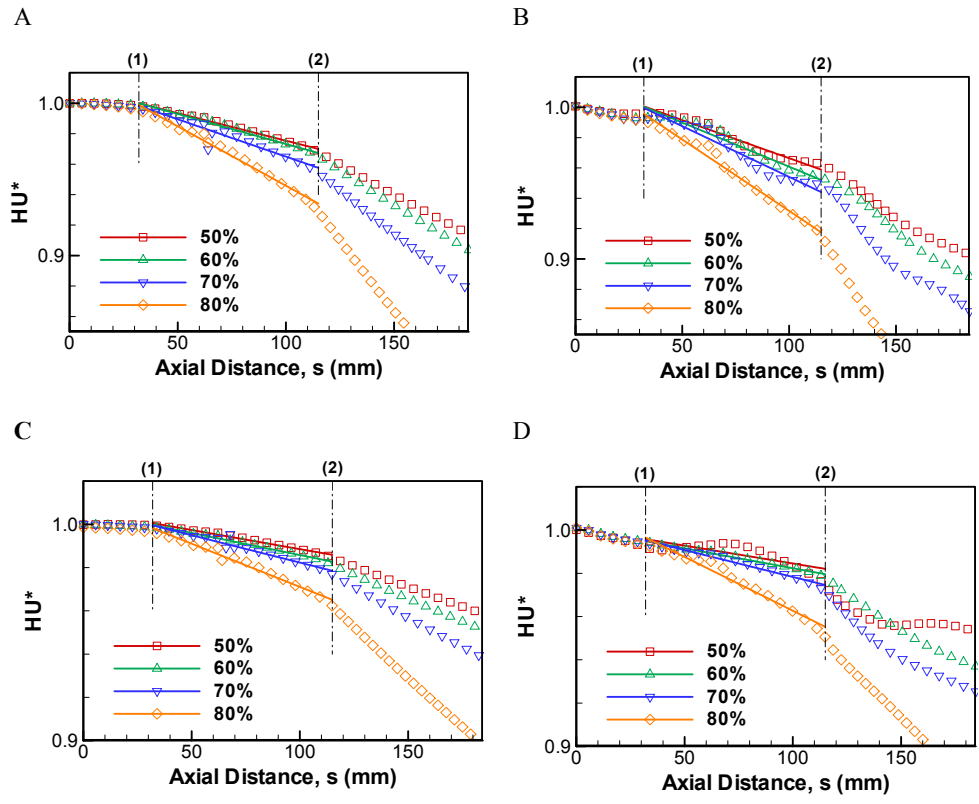


Figure 6. Normalized transluminal attenuation profiles along the axial direction of main arterial segment for (A) steady flow with $Q_n=50$ (ml/min) ($P_A = 3, P_B=0$ mmHg), (B) pulsatile flow with $Q_n=50$ (ml/min) ($P_A = 3, P_B=2.7$ mmHg), (C) steady flow with $Q_n=69$ (ml/min) ($P_A=4.5, P_B=0$ mmHg), and (D) pulsatile flow with $Q_n=69$ (ml/min) ($P_A=4.5, P_B=4.05$ mmHg). (1) and (2) indicate the locations of bifurcations shown in Fig 3. The attenuation profiles along the stenosed section (between (1)-(2)) are fitted by the linear function; $a \cdot s+b$ and the slope a represents the normalized TCG (TCG*). All the results are for the idealized model at the peak of AIF and the percentage refers to different area stenosis levels.

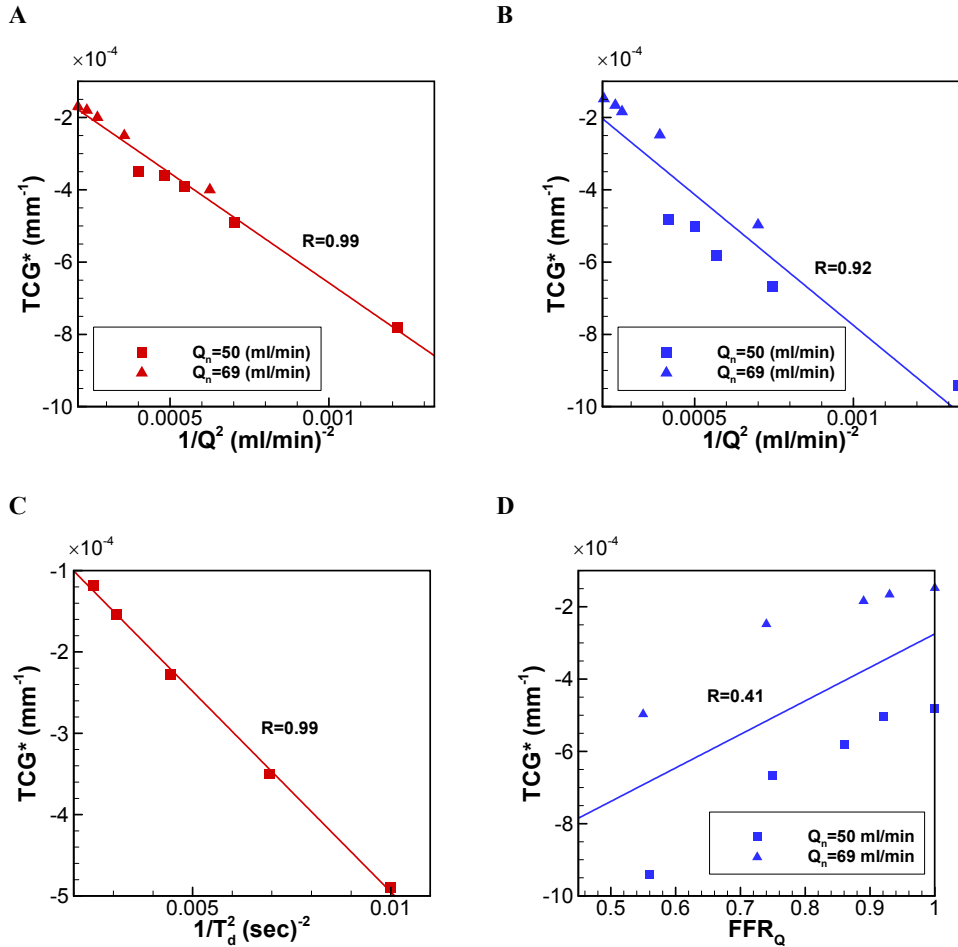


Figure 7. Correlation between (A) TCG and the inverse square of flow rate ($1/Q^2$) for steady flow, (B) for pulsatile flow, (C) TCG and the inverse square of bolus time, ($1/T_d^2$) for 70% stenosis and $Q_n=50$ ml/min, steady flow (D) TCG* and FFR_Q for pulsatile flow for the idealized model.

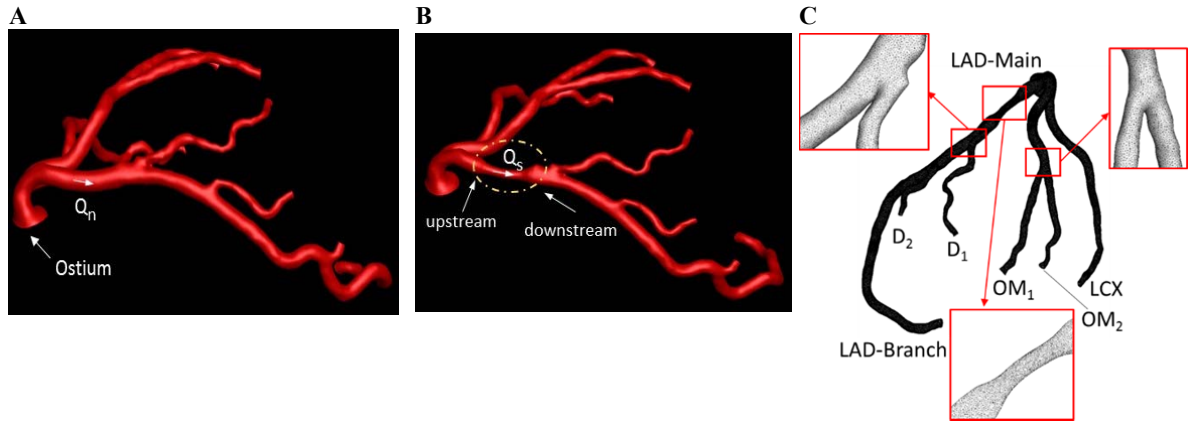


Figure 8. (A) 3-D model of a patient specific coronary artery for the normal (unstenosed) case. (B) Model of the artery with 70% stenosis. (C) Computational meshes employed in the various segments of the model.

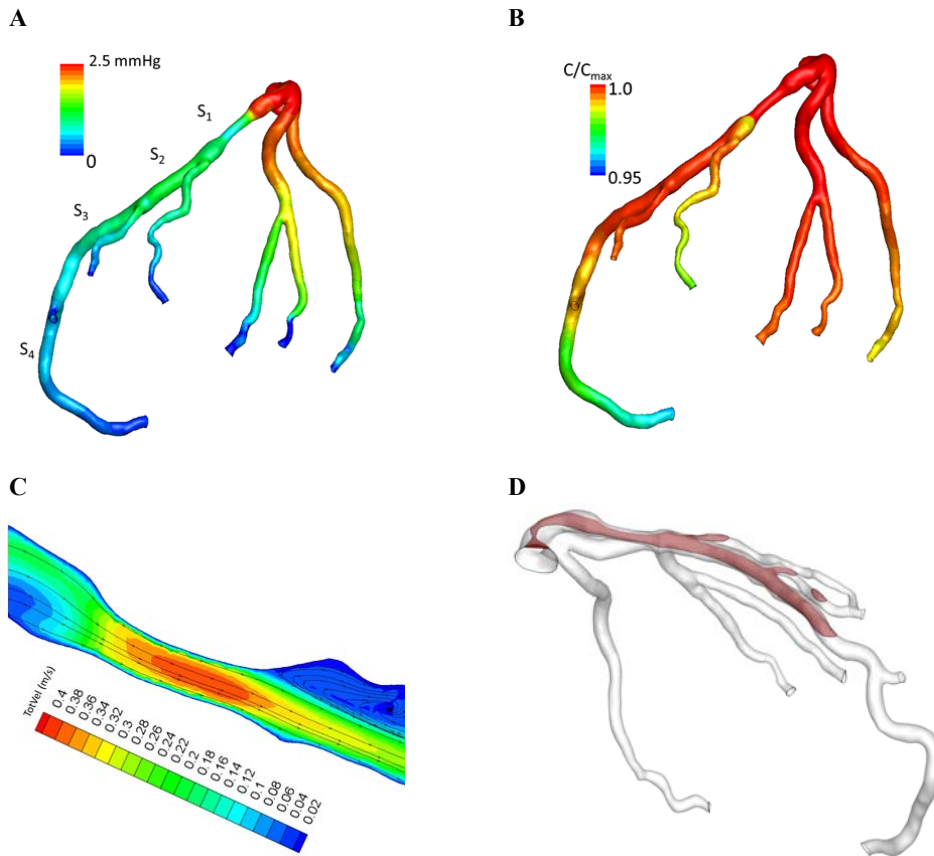


Figure 9. Patient specific computational results: Pressure (A), normalized contrast agent concentration (C/C_{max}) for the $Q_n=375$ ml/min case with a 70% area constriction. (B) and Velocity magnitude and streamlines in the stenosed region (C) cross sectional plane in which velocity contour in (C) is shown. The segmentations S_1 - S_4 are segments of the main LAD before each branch.

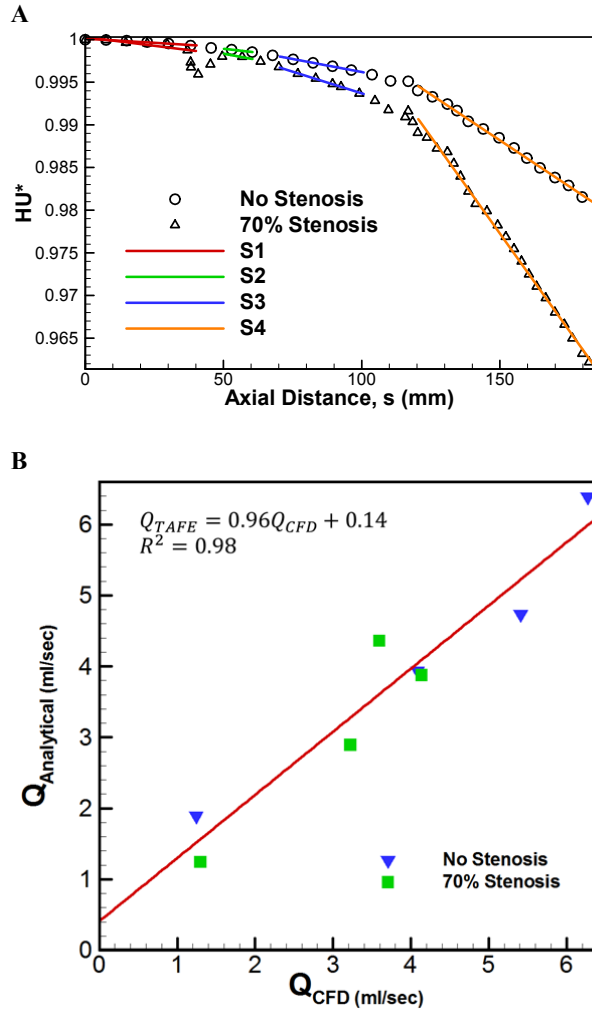


Figure 10. Patient specific normalized transluminal attenuation profiles along the axial direction of main arterial segment in LAD (steady flow) with $P_A=3$ and $P_B=0$ mmHg. (A) Correlation between CFD calculation of flow rate and TAFE calculation of the flow rate in the no-stenosis (normal) and 70% area stenosis cases (B).

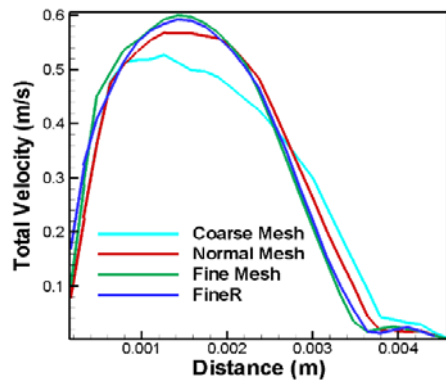
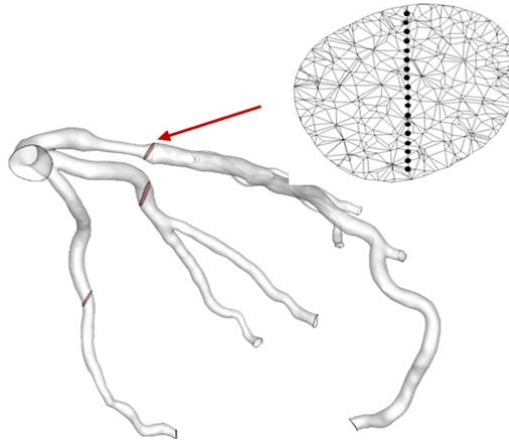
A**B**

Figure 11. (A) Patient Specific velocity magnitude profile comparison between different grid levels for the cross sections shown in (B) in red planes in the main LAD after the stenosis. (B) Cross section plane used in (A). The 4 different grid levels are ‘Coarse’ with $\approx 2 \times 10^5$, ‘Normal’ with $\approx 3 \times 10^5$, ‘Fine’ with $\approx 4.55 \times 10^5$ and ‘FineR’ with $\approx 9.25 \times 10^5$ tetrahedral elements.